

This is an Open Access document downloaded from ORCA, Cardiff University's institutional repository: <https://orca.cardiff.ac.uk/id/eprint/154482/>

This is the author's version of a work that was submitted to / accepted for publication.

Citation for final published version:

Manjunath, Ashwin Desai Belaguppa, Harid, Nouredine, Griffiths, Huw, Nogueira, Ricardo Pereira, Noyanbayev, Nurym, Haddad, Abderrahmane and Ramanujam, Sarathi 2023. Equivalent circuit models for soils and aqueous solutions under 2-terminal test configuration. IEEE Transactions on Electromagnetic Compatibility 65 (1) , pp. 225-234. 10.1109/TEMPC.2022.3216813

Publishers page: <http://dx.doi.org/10.1109/TEMPC.2022.3216813>







Please note:

Changes made as a result of publishing processes such as copy-editing, formatting and page numbers may not be reflected in this version. For the definitive version of this publication, please refer to the published source. You are advised to consult the publisher's version if you wish to cite this paper.

This version is being made available in accordance with publisher policies. See <http://orca.cf.ac.uk/policies.html> for usage policies. Copyright and moral rights for publications made available in ORCA are retained by the copyright holders.



Equivalent Circuit Models for Soils and Aqueous Solutions Under 2-Terminal Test Configuration

Ashwin Desai Belaguppa Manjunath , *Member, IEEE*, Nouredine Harid , Huw Griffiths, Ricardo Pereira Nogueira , Nuryim Noyanbayev , Abderrahmane Haddad , *Member, IEEE*, and Sarathi Ramanujam , *Senior Member, IEEE*

Abstract—Numerous circuit models have been proposed to represent the electrode–electrolyte interface (EEI) impedance and bulk medium impedance of conducting media. Following a review, two suitable models are constructed to represent the behavior of conduction in electrolytes and soils, respectively. Both models incorporate a constant phase element in parallel with an apparent Faradaic resistance, which is found to reproduce the EEI behavior accurately. For the electrolyte model, a single parallel R - C branch is added to represent the impedance of the bulk medium, whereas for the soil model, an equivalent ladder network of R - C branches is found to be suitable. Experimentally obtained electrolyte and soil impedance data based on 2-terminal impedance spectroscopy over a frequency range of 10 mHz to 10 MHz with variable current density are compared with values obtained from the models and where model parameters are determined by a curve fitting routine. The effects of electrolyte concentration, soil moisture, and electrode material are analyzed, and the models help to illustrate clearly how the EEI effect dominates at low frequencies while the intrinsic characteristics of the test medium prevails at high frequencies. The models are extended to account for soil–electrolyte impedance dependence on current density, which is most evident at low frequencies. The extent of the impedance plateau region is described by limiting upper and lower frequencies.

Index Terms—Circuit model, electrode–electrolyte interface (EEI), electrolytes, grounding, impedance, soil conduction.

I. INTRODUCTION

THE frequency dependence of soil electrical parameters is important for studying the lightning response of grounding systems and was the subject of recently published CIGRE WG C.4.33 [1]. The variation of soil resistivity (ρ) and permittivity (ϵ) with frequency [2], [3], [4], [5], [6], [7], [8], [9] has been

extensively studied, whereas dependence on current density and nonlinear metal–soil interfacial effects is relatively less explored. Earthing impedance can be measured with apparatus having test currents ranging only up to a few hundred milliamperes over a relatively low range of frequencies [10]. Particularly for instrumentation operating at low current levels, nonlinear interfacial effects can significantly affect measured values [11], [12], [13], [14]. These nonlinear effects at low frequency and low current density are recognized [15], [16], [17], but to date there has been limited work to account for such effects in electrical grounding applications.

A comprehensive review of frequency and current density dependence of soil parameters has been reported recently [18]. This study revealed wide variations in the published values of soil parameters with frequency (1 to 10^7 Hz) and these are attributed to different test setups, techniques, and soil types. Some investigators [2], [3], [19] reported very high values of permittivity (in the order of 10^6 to 10^8) at low frequencies, which may be due, for example, the electrode–electrolyte interface (EEI) effect [16], [20] and/or the electrical double layers formed within the bulk medium [5], [17], [21].

Here, a review of published equivalent circuit models for soils is presented and more representative refined equivalent circuits are proposed. The results of experiments presented in [18] on electrolyte samples and sand samples with varied conductivity and moisture content are used in this article. Given the complexity of the electrochemical processes with multi-ion solutions in the presence of metallic electrodes, and to separate the EEI behavior from that of the medium, single-salt Na_2SO_4 aqueous solutions were used, having mid-frequency resistivity matching that of common soils ($50 \Omega\cdot\text{m}$ – $10 \text{ k}\Omega\cdot\text{m}$). The samples were tested using two impedance measurement instruments to cover the required frequency and current density range, more details on the experimental procedure can be found in [18].

Accounting for both frequency and current density effects and using experimental data from Manjunath et al. [18], the model parameters are selected to obtain best fit. With such selection, it is found that, within the limits of frequencies and current densities used in this study, the proposed models closely reproduce the impedance response across the spectrum for the studied electrolytes and soils. The EEI contribution may explain some previously reported elevated values of apparent permittivity over low frequency ranges.

Manuscript received 18 March 2022; revised 25 May 2022 and 12 July 2022; accepted 14 July 2022. This work was supported by the Advanced Power and Energy Research Centre (APEC), Khalifa University, Abu Dhabi, UAE. (Corresponding author: Nouredine Harid.)

Ashwin Desai Belaguppa Manjunath, Nouredine Harid, Ricardo Pereira Nogueira, and Nuryim Noyanbayev are with the Khalifa University, Abu Dhabi 127788, United Arab Emirates (e-mail: ashwin.manjunath@ku.ac.ae; noureddine.harid@ku.ac.ae; ricardo.nogueira@ku.ac.ae; 100049398@ku.ac.ae).

Huw Griffiths and Abderrahmane Haddad are with the Cardiff University, Cardiff CF10 3AT, U.K. (e-mail: huw.griffiths@ku.ac.ae; haddad@cardiff.ac.uk).

Sarathi Ramanujam is with the Indian Institute of Technology Madras, Chennai 630036, India (e-mail: rsarathi@iitm.ac.in).

Color versions of one or more figures in this article are available at <https://doi.org/10.1109/TEMC.2022.3216813>.

Digital Object Identifier 10.1109/TEMC.2022.3216813

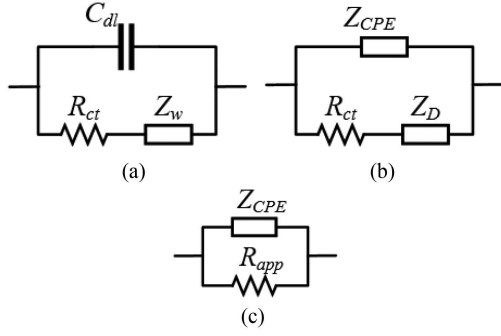


Fig. 1. EEI equivalent circuits (a) adapted from Randles [32], (b) adapted from Córdoba-Torres et al. [35], and (c) adapted from Engelhardt et al. [37].

II. REVIEW AND SELECTION OF EQUIVALENT CIRCUIT MODELS

Experimental impedance measurements in soils with the two-electrode arrangement include not only the impedance of the test medium itself but also that of the EEI. Interfacial effects are prominent at low frequencies depending on electrode material, soil moisture, and salt type and concentration.

A. Electrode–Electrolyte Interface Impedance

An electrode in contact with an electrolyte will develop a potential across the interface due to, inter alia, charge transfer between the electrode and the electrolyte. This charge separation or double layer comprises a complex EEI with several distinct properties [22], [23], [24].

Many equivalent circuit models, based on combinations of resistors and capacitors, have been developed to represent the EEI and its frequency dependence [24], [25], [26], [27], [28], [29], [30].

A commonly referenced model [31], [32] is shown in Fig. 1(a) where the Warburg impedance (Z_w), the impedance due to diffusion of ions in the electrolyte is placed in series with a charge transfer resistance (R_{ct}) representing the resistance to charge exchange between the electronic and the electrolytic conductors resulting from interface electrochemical reactions. This series combination is placed in parallel with the double-layer capacitance (C_{dl}). The Warburg effects manifest over a lower frequency range compared with the double-layer capacitance [33]. Usually, Z_w has a finite value at zero frequency due to the ubiquitous presence of oxides or adsorbed layers and, hence, it allows the passage of dc current [25] while $\text{Im}\{Z_w\}$ is proportional to $1/\sqrt{f}$. In these cases, Z_w can be replaced by a more generic diffusion impedance (Z_D). The double-layer capacitance C_{dl} is not constant as it reduces with frequency according to a power law and for reasons discussed in [34]. Such variation from ideal capacitive behavior is commonly represented by a constant phase element (CPE) impedance, Z_{CPE} [34], given by (1)

$$Z_{CPE} = Q^{-1} \cdot (j\omega)^{-a} \quad (1)$$

where Q and a are constants.

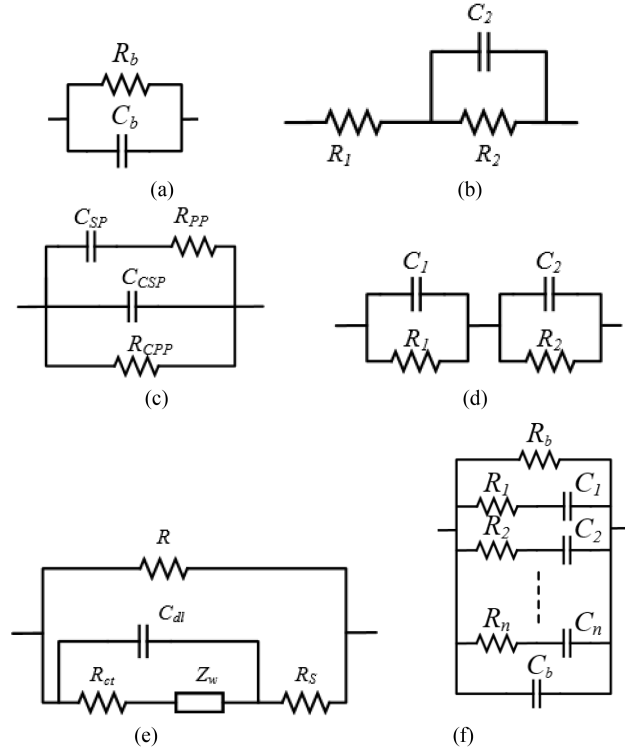


Fig. 2. Bulk material equivalent circuits (a) for pure electrolyte adapted from the work in [23] and (b)–(f) for soils adapted from the works in [39], [40], [43], [42], and [44], respectively.

The resulting EEI model with Z_{CPE} and Z_D is shown in Fig. 1(b) [35]. In some cases, under a limited range of low frequency investigation, the contribution of the diffusion element may not be clearly identified in the response. Then, the diffusion impedance may be omitted, and the charge transfer resistance combined with other contributing resistances yielding an overall apparent resistance R_{app} with a model, as shown in Fig. 1(c) [36], [37].

B. Bulk Medium Impedance

1) *Electrolytes*: As frequency increases beyond a certain value, the EEI impedance becomes negligible, and the system response is governed by the behavior of the electrolyte only. In the case of a single-salt solution and as proposed in [23], the electrolyte exhibits both conductive and capacitive behaviors, which can be represented by a resistor, R_b , in parallel with a capacitor, C_b , as shown in Fig. 2(a). For a conducting medium of uniform cross-sectional geometry, these circuit parameters can be calculated with the following equations:

$$R_b = \frac{d}{\sigma A} \quad (2)$$

$$C_b = \frac{\varepsilon_0 \varepsilon_r A}{d} \quad (3)$$

where A is the area of the electrodes, d is the distance between the electrodes, σ is the resistivity of plateau region [18], and ε_r

is the relative permittivity of water, which is assumed constant (~ 80) over the entire frequency range in this study [18], [38].

2) *Soils*: In the case of soils, a more complex high-frequency response with multiple relaxations is obtained, as will be shown in Section III-B. Such response is governed by combined contributions of the solid material, the multi-ion electrolyte in the pores, and the interfaces between the solid material and electrolyte. Many equivalent circuits for soils have been proposed [4], [31], [39], [40], [41], [42], [43], [44]; for example, as shown in Fig. 2(b), Gu et al. [39] propose a circuit model comprising a resistance R_1 in series with a parallel combination of resistance R_2 and capacitance C_2 to represent different phases of the material. Song [40] and Han et al. [43] adopted a model with three parallel branches representing separate paths within the soil: (i) a capacitance C_{SP} in series with a resistance R_{PP} – the discontinuous soil particle-pore path, (ii) a capacitance C_{CSP} – the continuous soil particle path, and (iii) a resistance R_{CPP} – the continuous pore path, as shown in Fig. 2(c). A simplified model was proposed consisting of two R - C parallel branches [see Fig. 2(d)] [40], [43], whereas Dias [31], [42] introduced a model to account for interface effects that commonly feature with clays [21], [45]. Such clay-electrolyte membrane interface effects within the bulk of the sample [see Fig. 2(e)] are modeled by a Warburg-type circuit [c.f. Fig. 1(a)] in series with R_S representing the homogenous portion of electrolyte. That series circuit is placed in parallel with a resistance R accounting for parallel conduction through an unblocked pore and/or a pore wall. Alternatively, an R - C ladder network was proposed as a circuit equivalent for soils, as shown in Fig. 2(f) [44]. In this figure, R_b represents the dc resistance of the bulk medium, whereas C_b represents the capacitance at infinite frequency. The multiple R_n - C_n series branches provide responses with various time constants characterizing multiple relaxations with frequency [44] and where the number of R - C branches n is determined from the order of the frequency response from a polynomial fit.

C. Adopted Models

In this article, two models are adopted with elements combined to represent the bulk medium and the soil-electrode interface effects, as shown in Fig. 3. Since the concepts of electrochemical theory apply to any electronic conductor exposed to an ionic conductor, as is the case with soil energized with metallic electrodes, these concepts are used here to explain the interface effects. Electrode polarization can occur in a wide frequency range from 1 mHz to 100 kHz and may lead to measurement results that are far from the true/intrinsic characteristics of the medium. It is particularly evident in the case of interfaces between metal oxides and wet or partially saturated soil. When an electronic conductor, typically a metal, is immersed in an electrolyte, a spontaneous spatial arrangement of the different charge carriers at both sides of the interface—electrons at the metal side and ions at the electrolyte—occurs. This opposite charge distribution forms the so-called electrical double layer at the electrode-electrolyte interface or EEI, as shown in Fig. 3(a). Hence, an intrinsic electrochemical potential and an impedance

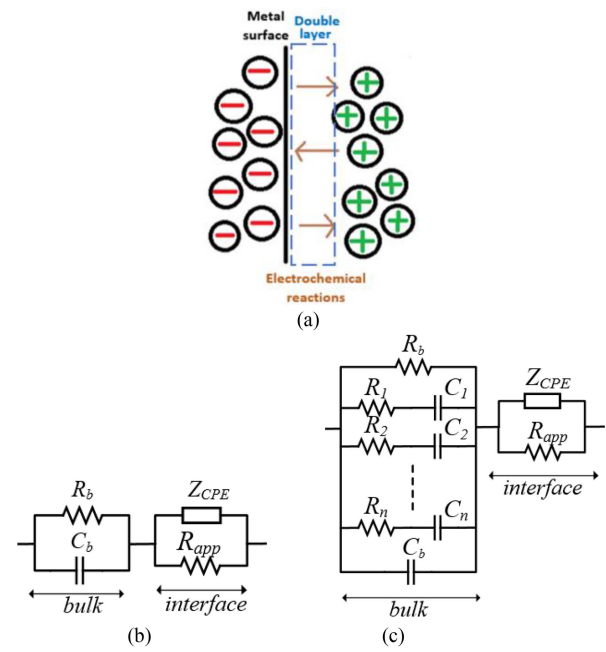


Fig. 3. (a) Double layer at the interface and adopted circuits for (b) single-salt electrolyte and (c) soil.

that is current density and frequency-dependent may be used to characterize the double layer. These interface effects are modeled here by a parallel combination of a CPE representing the electric double-layer nonideal capacitance effect and an apparent resistance R_{app} . This apparent overall resistance encompasses the charge transfer resistance and the eventual low-frequency limit of faradaic reactions as oxide formation or intermediate species adsorption occurring at the interface. Fig. 3(b) represents the case when the conducting medium is a single-salt electrolyte and where the bulk impedance can be represented by a simple parallel R - C circuit. In the case of soils, as shown in Fig. 3(c), the same representation is used for the interface effects, but an n -branch R - C ladder network represents the bulk medium to account for the nonideal high-frequency response with multiple relaxations seen in multi-ion soils, with R representing the bulk medium resistance and C the bulk medium capacitance. It will be shown that the low-frequency responses seen in the Nyquist plots are well represented by such models.

Expressions for the impedances of the elements are given in (4)–(9). The circuit parameters R_b and C_b of the bulk medium are calculated using (2) and (3), and the other circuit parameters (Q , a , R_{app} , R_n , and C_n) are determined by fitting to the measured impedance spectroscopy data [46]

$$Z_{elec} = \frac{R_b}{1 + \omega^2 R_b^2 C_b^2} + \frac{R_{app} x_1}{x_1^2 + y_1^2} + j \left(\frac{R_b^2 C_b}{1 + \omega^2 R_b^2 C_b^2} + \frac{R_{app} y_1}{x_1^2 + y_1^2} \right) \quad (4)$$

$$Z_{soil} = \frac{x}{x^2 + y^2} + \frac{R_{app} x_1}{x_1^2 + y_1^2} + j \left(-\frac{y}{x^2 + y^2} + \frac{R_{app} y_1}{x_1^2 + y_1^2} \right) \quad (5)$$

$$x = \frac{1}{R_b} + \sum_1^n \frac{\omega^2 R_n C_n^2}{1 + \omega^2 R_n^2 C_n^2} \quad (6)$$

$$y = \omega C_b + \sum_1^n \frac{\omega C_n}{1 + \omega^2 R_n^2 C_n^2} \quad (7)$$

$$x_1 = 1 + Q\omega^a \cos\left(\frac{\pi a}{2}\right) R_{app} \quad (8)$$

$$y_1 = Q\omega^a \sin\left(\frac{\pi a}{2}\right) R_{app}. \quad (9)$$

The frequency dependence of impedance enables interpretation of the soil's response to variable-frequency current flow by the proposed equivalent circuits. An intuitive correlation between the measured impedance spectroscopy data and discrete electrical components of the equivalent circuit will help understand the underlying behavior of the medium and EEI effect. From the expression for impedance (4) and (5), the model impedance response can be calculated, and from the calculated impedance, $\sigma(\omega)$ and $\varepsilon(\omega)$ can be obtained with known geometry.

Current density dependence of the EEI branch is modeled by replacing R_{app} and Q with current density functions $R_{app}(J)$ and $Q(J)$ as will be shown later. Since only ac behavior is explored, the "half-cell potential" is not included in the proposed models.

III. EXPERIMENTAL RESULTS AND DISCUSSION

Impedance spectroscopy measurements in the range 10 mHz to 10 MHz at current densities between 1 and 600 mA·m⁻² were made on deionized water, diluted electrolyte (Na₂SO₄), and soil (sand) samples placed in a cuboid test cell. Sample solution concentrations and soil moistures were varied from 0.01 to 1 mM and from 0 to 2.6 wt.%, respectively, to encompass matching wide-range values of practical soils. Four different electrode metals were used: copper, stainless steel, aluminium, and platinized titanium. The details of the experimental procedure, instrumentation, data acquisition system, and results are given in [18].

A. Bode Plots With Electrolyte and Sand Test Medium

Selected results are presented from tests carried out on two test media using Pt electrodes. Fig. 4(a) and (b), respectively, shows the impedance magnitude and phase angle variations with frequency for both 0.1-mM Na₂SO₄ electrolyte solution and 1wt.% moisture sand. Similar trends are seen for the other electrolyte solution concentrations and sand samples of different moisture content, and with the different electrode materials. Over a low frequency range, both test media exhibit elevated values of impedance, which is attributed to the EEI effect. However, this low frequency impedance increase was found to be much more significant and extensive in the case of the sand samples, which may be due to (i) a less strong contact of sand with the electrodes compared with pure electrolyte, (ii) the hindered ionic mobility in sand, and (iii) the fact that the electrolytic solution in sand is multi-ionic [18]. Beyond the frequency region where the EEI is influential, a plateau region is observed with a near to zero phase angle, over a wide frequency

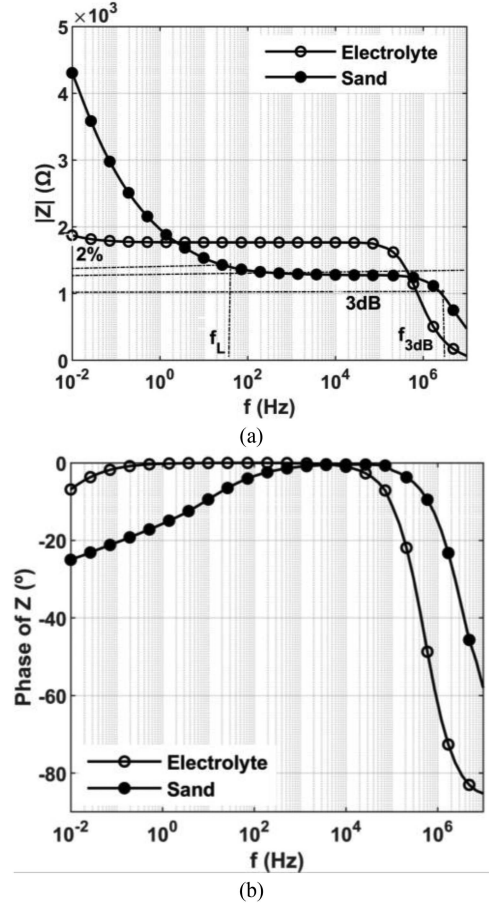


Fig. 4. Typical measurements of (a) impedance magnitude and (b) phase angle.

range in the case of electrolytes, due to ionic conduction in the bulk medium. As the frequency further increases beyond the plateau, a fall in impedance is observed and accompanied by an increasing leading phase angle indicating an increase in displacement current. Variation of impedance magnitude with frequency is quantified in terms of defined frequency thresholds. The lower limit f_L is the frequency at which the impedance magnitude is 2% above the average plateau value and f_{3dB} , referred to as a downturn frequency, is the value at which the impedance magnitude decreases by 3 dB below its average plateau value.

It was found experimentally that a small amount of stray inductance in the test setup (~ 400 nH) affects results to some extent in the high frequency range for high conductivity media and the results have been corrected accordingly. To estimate the inductance of the measurement circuit, the two aluminum test cell plates were shorted with nine aluminum rods of 20-mm diameter distributed equidistantly on each plate. Tests were made to measure the impedance across the frequency range 1 Hz–40 MHz using the Bode instrument 100 [18] of (i) the shorted test cell and connecting wires and (ii) the connecting wires and cables only (cable terminals connected together with test cell removed). The resistance and inductance in each case

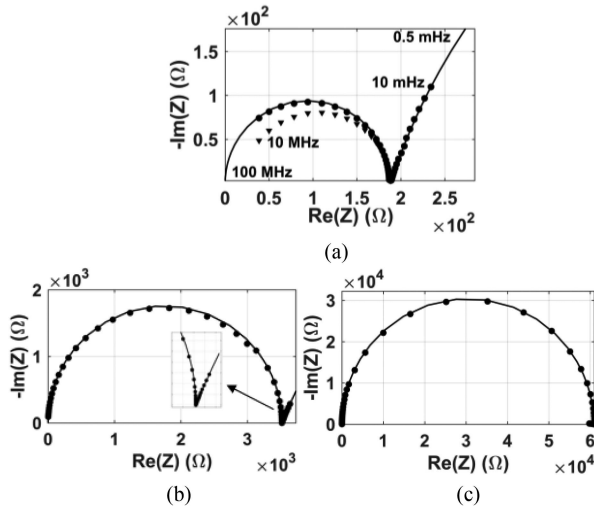


Fig. 5. Nyquist plots of experimental data and circuit model response: Pt electrodes and (a) 1-mM solution, (b) 0.05-mM solution, and (c) DI water. ▼ experimental data without correction for stray inductance.

TABLE I
MODEL PARAMETERS FOR DIFFERENT SOLUTIONS WITH PT ELECTRODES

| Solution /Concentration | Model parameters | | | | |
|----------------------------|------------------|---------------|-------------------|--|------|
| | R_b (kΩ) | C_b (pF) | R_{app} (kΩ) | Q ($10^{-3} \cdot S \cdot s^a$) | a |
| DI water | 60.98 | 162 | - | - | - |
| 0.01mM | 12.53 | 162 | 1.30 | 25.12 | 0.71 |
| 0.05mM | 3.52 | 162 | 5.01 | 26.54 | 0.78 |
| 0.1mM | 1.77 | 162 | 9.05 | 33.95 | 0.76 |
| 1mM | 0.19 | 162 | 1.37 | 74.56 | 0.80 |

circuit are derived from the real and imaginary parts of the measured impedance assuming a series R - L circuit representation. Both setups yielded an inductance of (~ 400 nH), showing that the cell inductance is negligible, and the circuit inductance is mainly due to connecting wires. A value of 400 nH is adopted for inductance correction.

In the following section, a series of selected experimental results are shown as Nyquist plots, which assist with interpretation of the frequency response of the proposed models. The experimental results and fitted circuit model curves are presented first for the pure electrolytes, followed by those for various soil test media. The effect of electrode material is considered and, finally, current density dependence is modeled.

B. Nyquist Plots and Fitted Equivalent Circuit Parameters

1) *Electrolyte Solutions of Different Concentration:* Fig. 5(a)–(c) shows Nyquist plots of selected experimental data (dots) and the corresponding circuit model values [based on Fig. 3(a)] (solid lines) for Na_2SO_4 electrolyte of different concentrations with Pt electrodes. Table I shows the fitted model parameter values, R_{app} , Q , and a , calculated using a MATLAB routine based on Nelder–Mead simplex direct search algorithm [46], and the calculated values of R_b and C_b from (2) and (3). The Nyquist plots enable distinct high- and low-frequency

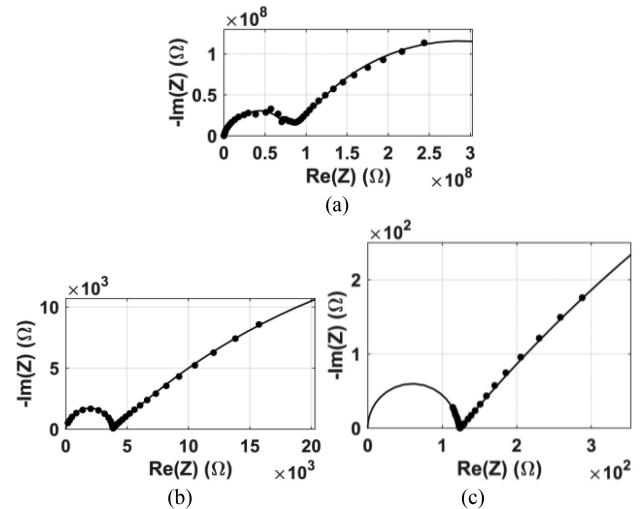


Fig. 6. Nyquist plots of experimental data and circuit model response: Pt electrodes and (a) dry sand, (b) 0.55 wt.% sand, (c) 2.6 wt.% sand.

regions relating to the bulk and EEI response, respectively, to be visualized. In Fig. 5(a), the limiting frequencies of the model and experimental test range data are identified, and these two regions are quite distinct. First, a high-frequency arc is evident; here, the circuit model predicts an ideal semicircular curve and intersection at high frequency with the origin, closely reproducing the experimental data. The results obtained without stray inductance correction deviate from the ideal curve. Second, the low frequency region is identified as an arc, and the model and experimental results agree closely. For the lower concentration solution, the arc corresponding to the EEI effect is less pronounced [see Fig. 5(b)], whereas for deionized water, no clear EEI response can be gleaned [see Fig. 5(c)].

2) *Sand Samples of Different Moisture Content:* Fig. 6(a)–(c) shows corresponding Nyquist plots for dry sand and sand with two different moisture contents energized with Pt electrodes. From the figures, it can be seen that the bulk and EEI response regions can be identified, and it is seen that the EEI effect is generally more extensive in sand compared with electrolytes of corresponding similar bulk impedance values. The extent of the EEI response relative to bulk response increases with moisture. The experimental EEI response in these tests can be modeled accurately by a curve obtained using the CPE element in parallel with a constant apparent resistance. Unlike the high frequency bulk responses for the Na_2SO_4 electrolytes, those of sand samples shown in Fig. 6 are not a perfect semicircle, notably at low moisture content.

To model this response more accurately, a fourth-order polynomial fit based on three parallel R - C branches was used. The corresponding parameters of the equivalent circuit model are given in Table II, and the values of R_b calculated from (2). The plateau value of conductivity, determined by soil moisture content, is used [18]. The value of cell capacitance varies with moisture and is calculated with (3) using the high frequency (10 MHz) value of ϵ_r [18]. Fig. 6 shows that the model reproduces closely the measured data for all moisture contents within the test frequency limits.

TABLE II
MODEL PARAMETERS FOR SAND SAMPLES OF DIFFERENT MOISTURE CONTENT WITH Pt ELECTRODES

| Moisture (wt.%) | R_b (k Ω) | C_b (pF) | R_l (k Ω) | C_l (pF) | R_2 (k Ω) | C_2 (pF) | R_3 (M Ω) | C_3 (pF) | R_{app} (M Ω) | Q ($10^{-3} \cdot S \cdot s^a$) | a |
|-----------------|---------------------|------------|---------------------|------------|---------------------|------------|---------------------|------------|-------------------------|-------------------------------------|------|
| 0 | $85.50 \cdot 10^3$ | 9.82 | $4.66 \cdot 10^5$ | 76.50 | $70.94 \cdot 10^3$ | 16.90 | 7.58 | 8.61 | 405 | $2.18 \cdot 10^{-5}$ | 0.66 |
| 0.25 | 38.04 | 25.36 | 994.00 | 8.05 | 7.63 | 10.70 | 0.86 | 44.70 | 0.61 | 0.02 | 0.44 |
| 0.55 | 3.85 | 28.30 | 28.99 | 6.94 | 2.13 | 9.56 | 0.23 | 43.60 | 0.07 | 0.22 | 0.49 |
| 1 | 1.29 | 29.54 | 34.10 | 6.07 | 1.50 | 10.01 | - | - | 0.01 | 0.89 | 0.48 |
| 2.6 | 0.12 | 29.75 | 3.60 | 15.00 | - | - | - | - | $3 \cdot 10^{-3}$ | 18.50 | 0.56 |

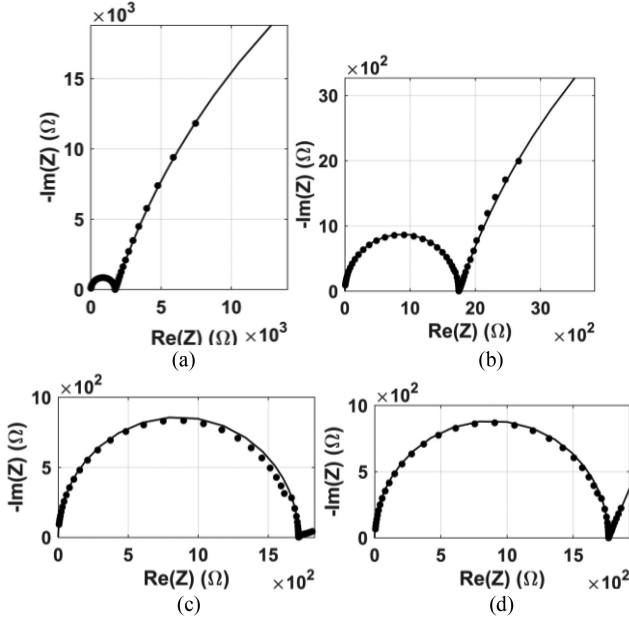


Fig. 7. Nyquist plots of experimental data and corresponding circuit model data for 0.1-mM solution with (a) Al electrodes, (b) SS electrodes, (c) Cu electrodes, and (d) Pt electrodes.

3) *Effect of Electrode Material*: In two-terminal and three-terminal measurements of soil, the potential is measured between the reference and the metallic electrodes, which means that the type of electrode material affects the measured soil/electrolyte impedance at low frequency and efforts are made to minimize the EEI effect, accordingly [25], [29]. As a result, Pt electrodes are widely used in different domains of engineering applications, as they present low EEI impedance [47]. Figs. 7 and 8 show Nyquist plots for a constant electrolyte concentration and soil moisture, respectively, tested with different electrode materials. As expected, the EEI effect evident over the low frequency range is significantly different for the different electrode materials, whereas the bulk response is the same.

The EEI effect can be ranked in order of position of the materials in the reactivity series: aluminium, steel, copper, and platinum. The equivalent circuit parameters determined for the electrolyte and soil models are shown in Tables III and IV, respectively. The calculated values of R_b and C_b show slight variations due to small differences in test solution and sand sample preparation.

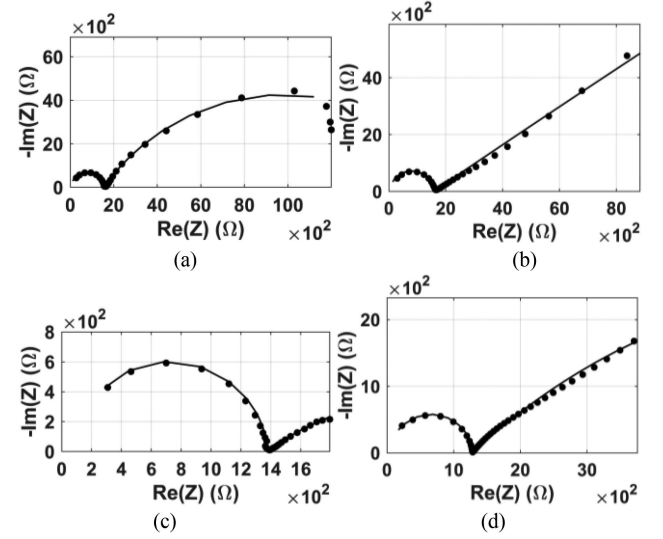


Fig. 8. Nyquist plots of experimental data and corresponding circuit model data for 1wt% sand with (a) Al electrodes, (b) SS electrodes, (c) Cu electrodes, and (d) Pt electrodes.

TABLE III
MODEL PARAMETERS FOR 0.1-mM SOLUTIONS WITH DIFFERENT ELECTRODES

| Electrode material | Model parameters | | | | |
|--------------------|---------------------|------------|-------------------------|-------------------------------------|------|
| | R_b (k Ω) | C_b (pF) | R_{app} (k Ω) | Q ($10^{-3} \cdot S \cdot s^a$) | a |
| Al | 1.73 | 162 | 97.04 | 0.65 | 0.80 |
| SS | 1.75 | 162 | 20.0 | 3.89 | 0.79 |
| Cu | 1.72 | 162 | 0.28 | 21.19 | 0.42 |
| Pt | 1.77 | 162 | 9.05 | 33.95 | 0.76 |

4) *Effect of Mid-Frequency Test Medium Resistivity on Frequency Cut off Points*: It is noted in [18] that impedance magnitude (and reflected in calculated apparent resistivity and permittivity) is characterized by a mid-frequency plateau flanked either side by two nonlinear regions occupying low and high frequency ranges; an example of which is shown in Fig. 4(a). It is also noted that the frequency limits of the plateau region shift according to different values of mid-range bulk soil resistivity. Here, such variation with frequency is quantified in terms of defined limits. The lower limit f_L , taken as the frequency at which the impedance magnitude is 2% above the average plateau value and

TABLE IV
MODEL PARAMETERS FOR 1WT% SAND SAMPLES WITH DIFFERENT ELECTRODES

| Electrode material | R_b (k Ω) | C_b (pF) | R_l (k Ω) | C_l (pF) | R_2 (k Ω) | C_2 (pF) | R_{app} (k Ω) | Q ($10^{-3} \cdot S \cdot s^a$) | a |
|--------------------|------------------------|---------------|------------------------|---------------|------------------------|---------------|----------------------------|--|------|
| Al | 1.53 | 29.55 | 24.63 | 11.97 | 0.32 | 51.20 | 16.53 | 0.20 | 0.61 |
| SS | 1.58 | 29.30 | 24.89 | 11.92 | 0.30 | 52.30 | 655.50 | 0.29 | 0.38 |
| Cu | 1.38 | 29.35 | 25.35 | 11.75 | 0.30 | 50.01 | 2.31 | 5.25 | 0.41 |
| Pt | 1.29 | 29.54 | 24.10 | 11.90 | 0.28 | 49.10 | 12.9 | 0.89 | 0.48 |

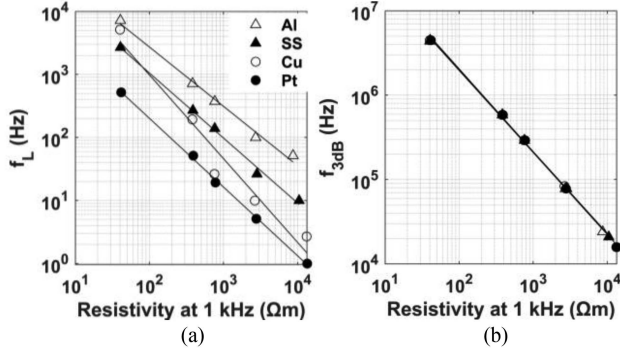


Fig. 9. Variation of (a) f_L and (b) f_{3dB} with resistivity at 1 kHz for different electrodes.

f_{3dB} may be referred to as a downturn frequency [see Fig. 4(a)]. Fig. 9(a) shows that f_L falls with mid-range resistivity (value taken at 1 kHz) for electrolyte solutions according to a linear relationship. The EEI effect is larger for Al and SS electrodes, and consequently shows higher values of f_L compared to Cu and Pt electrodes, probably due to the presence of passive films on the surface of the electrodes (self-protective metal oxide layers spontaneously formed upon the metallic surface). Fig. 9(b) shows that f_{3dB} follows a similar trend with mid-range resistivity and is independent of the electrode material. This corresponds to the fact that f_{3dB} is determined by the cell capacitance (C_b) and bulk resistance (R_b), and it is given by $f_{3dB} = 1/(2\pi R_b C_b)$.

C. Current Density Dependence of Impedance

The effect of current density on the measured impedance was explored by testing samples over a range of increasing voltages using an in-house developed impedance measurement system (IMS) [18]. A test frequency range from 0.5 Hz to ~ 2 kHz was adopted. Here, results are shown for tests carried out on two media: (i) a 0.05-mM Na_2SO_4 solution, and (ii) a 0.55 wt.% sand sample. In both tests, stainless steel electrodes were used. The measured variations of the test cell impedance of the two samples with current density and with frequency are shown in Fig. 10(a) and (b). From the figures, it can be observed that impedance decreases with current density increase, and the rate of decrease is higher at lower frequencies.

The impedance data in Fig. 10(a) and (b) were fitted using second-order power equations from which interpolated values were used to construct constant current density curves. Accordingly, the variation of impedance with frequency at constant

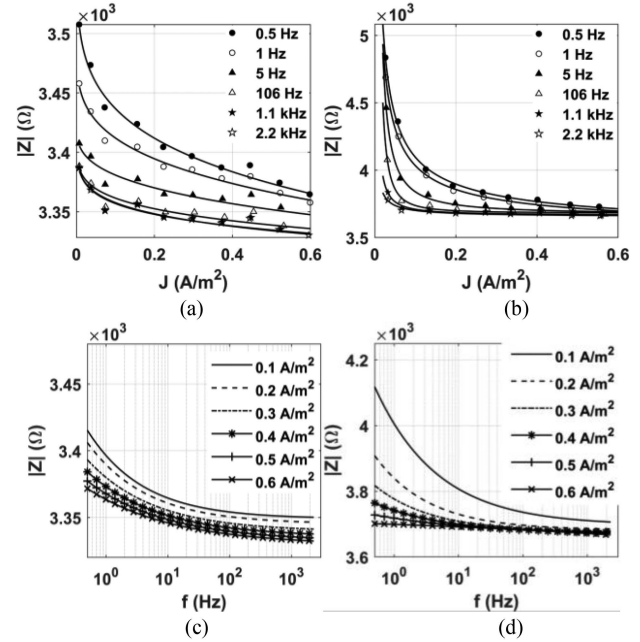


Fig. 10. Effect of current density at constant frequency: (a) electrolyte and (b) sand. Effect of frequency at constant current density: (c) electrolyte and (d) sand.

TABLE V
VALUES OF THE CONSTANT USED IN (11)

| f (Hz) | Electrolyte | | Sand | |
|---------------------|-------------|------|--------|------|
| | m | n | m | n |
| 0.5 | 69.21 | 0.23 | 135.30 | 0.62 |
| 1 | 63.07 | 0.19 | 110.10 | 0.65 |
| 5 | 49.25 | 0.17 | 10.50 | 1.22 |
| 106 | 36.12 | 0.19 | 1.20 | 1.66 |
| $1.1 \cdot 10^{-3}$ | 31.81 | 0.21 | 3.05 | 1.16 |
| $2.2 \cdot 10^{-3}$ | 32.06 | 0.20 | 4.91 | 0.97 |

current density can then be expressed, as shown in Fig. 10(c) and (d). The EEI current density effect is more prominent for sand samples compared with electrolytes. The impedance–current density relationship at a given frequency (f_i) is found to follow a power equation relation (10):

$$Z(J, f_i) = Z_0 + mJ^{-n} \quad (10)$$

where Z_0 is the asymptotic value of Z , and m and n are constants for a given test medium at frequency f_i . Table V gives values of

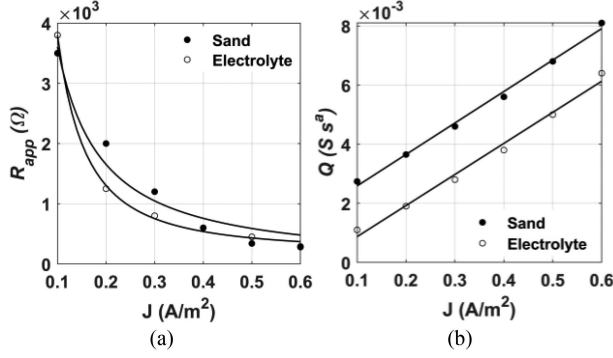


Fig. 11. Variation of (a) R_{app} and (b) Q with current density for 0.05-mM solution and 0.55 wt. % sand with solid lines indicating equation fits.

TABLE VI
VALUES OF THE CONSTANTS USED IN (12) AND (13)

| Medium | c | d | e | k |
|------------------|--------|------|------|---------------------|
| 0.05 mM solution | 70.61 | 1.71 | 0.01 | $4 \cdot 10^{-4}$ |
| 0.55 wt% sand | 270.30 | 1.12 | 0.01 | $1.5 \cdot 10^{-3}$ |

the constant m and n for 0.05-mM solution and 0.55 wt.% sand with SS electrodes.

By fitting the circuit models to the experimental data obtained at constant current densities, the curves giving the variations of R_{app} and Q with current density can be constructed, and these are shown in Fig. 11. The relationship between R_{app} and J can be assumed to follow approximately a power law according to (11), whereas parameter Q follows a linear trend given by (12)

$$R_{app}(J) = R_{app0} + cJ^{-d} \quad (11)$$

$$Q(J) = eJ + k \quad (12)$$

where R_{app0} is the asymptotic value of equivalent EEI resistance with current density and c , d , e , and k are constants that are given in Table VI for the electrolyte and sand media. These equations are applicable for both electrolyte and sand with different salt concentrations and moisture content, respectively, for the range of tested current densities.

Substituting the values of R_{app} and Q in (11) and (12) into (4), (5), (8), and (9), the impedance values as a function of both frequency and current density are calculated. The computed Nyquist plots obtained after incorporating the current-density dependent parameters in the model are presented in Fig. 12, showing reasonably good fit with measured data across a wide range of current density values.

For the selected electrolyte salt solution, the electrolyte model results conform very well with the measured EEI response obtained both with the Gamry instrument [see Fig. 12(a)] and the IMS instrument [see Fig. 12(c)] while the bulk response remains unchanged. An equally good fit with the EEI response is obtained with the selected sand medium. With high current densities, the EEI responses of sand are less dependent on current density than the responses of the electrolytes, as shown in Fig. 12(d). In Fig. 12(c) and (d), only the EEI response is shown because the

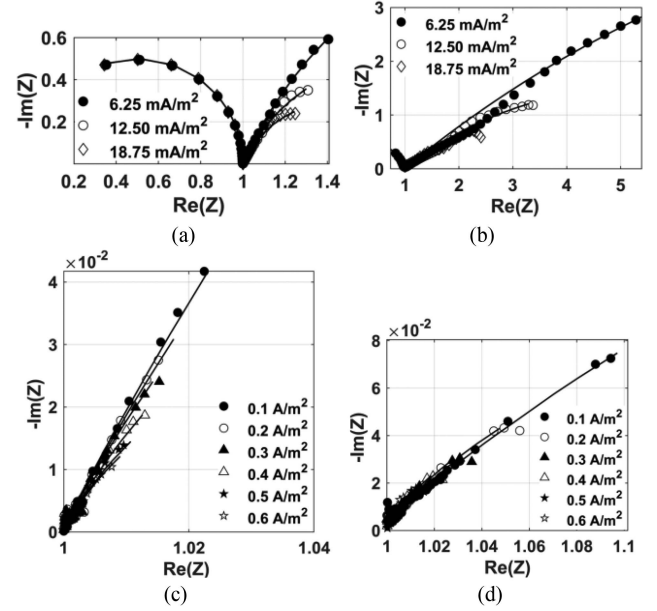


Fig. 12. Nyquist plots of normalized experimental data and corresponding circuit model data with SS electrodes for (a) 0.05-mM solution with Gamry, (b) 0.55 wt.% sand with Gamry, (c) 0.05-mM solution with IMS, and (d) 0.55 wt.% sand with IMS. Values normalized to plateau region impedance magnitude.

IMS system has limited frequency range and because only this response is affected by current density.

IV. CONCLUSION

Equivalent circuit models have been developed to reproduce the measured impedance spectroscopy results for electrolytes and soils, including the effect of current density dependence over the low frequency range. The findings indicate that the following.

- 1) The circuit model that provides a good fit for the experimental data for aqueous solutions consists of a parallel $R-C$ branch to represent the bulk behavior of the system in series with a parallel combination of constant-phase element and apparent resistance to represent the EEI.
- 2) For soils with varying moisture content, the same EEI circuit can be used in series with a ladder $R-C$ network.
- 3) The extent of the EEI response relative to the bulk response increases with moisture content and electrolyte salt concentration.
- 4) The EEI effect is relatively low for copper and platinized titanium electrodes but significantly higher for stainless steel and aluminum for both soil and electrolyte samples.
- 5) The current density dependence was accounted for in the proposed models by using current-density-dependent apparent charge transfer $R_{app}(J)$ and $Q(J)$ with defined relationships.
- 6) The boundaries of the plateau regions of impedance were described by limiting frequencies: (i) a lower frequency, (f_L), up to which the EEI effect lasts, and (ii) an upper frequency, f_{3dB} , corresponding to the $-3dB$ point of the

response. f_L and f_{3dB} were found to decrease with resistivity for all electrodes. The lower limit f_L is dependent on of the electrode material while f_{3dB} is not.

- 7) The proposed models provide good reproduction of the variation of measured impedance with frequency and current density for two-terminal tests for electrolytes and soils. The results suggest that the EEI impedance accounts for the marked increases in capacitive impedance over a significant low frequency range.
- 8) In grounding system measurements with two terminal configurations, the measured impedance is influenced by the electrode–electrolyte interface effect at low frequency. This article shows how such effects are analyzed through an equivalent circuit approach so that the measured impedance can be corrected accordingly.
- 9) The density of the applied test current influences the measured impedance significantly. Both the CPE and the apparent resistance representing the interface impedance show a decrease in magnitude with increasing current density. This has important implications in practice and needs to be taken into consideration when testing with low current instruments.
- 10) Further tests are required on the same test samples using the four-terminal test configuration and with clay soil, which may exhibit internal EEI effects.

REFERENCES

- [1] "Impact of soil-parameter frequency dependence on the response of grounding electrodes and on the lightning performance of electrical systems," CIGRE WG C4.33, Tech. Brouchure- 781, 2019.
- [2] R. L. Smith-Rose, "The electrical properties of soil for alternating currents at radio frequencies," *Proc. Roy. Soc. London*, vol. A-140, pp. 359–377, 1932.
- [3] G. V. Keller and P. H. Licastro, *Dielectric Constant and Electrical Resistivity of Natural-State Cores*. Denver, CO, USA: U.S. Dept. Interior, Geological Surv., 1959, pp. 1052–105H.
- [4] C. L. Longmire and K. S. Smith, "A universal impedance for soils," Defense Nucl. Agency, Washington, DC, USA, Rep. DNA 3788T, 1975.
- [5] W. R. Eberle, "The effects of water content and water resistivity on dispersion of resistivity and dielectric constant in quartz sand in the frequency range 10^2 - 10^8 Hz," U.S. Dept. Interior Geological Surv., Denver, CO, USA, Open-File Rep. 83-914, 1983.
- [6] A. A. Garrouh and M. M. Sharma, "The influence of clay content, salinity, stress, and wettability on the dielectric properties of brine-saturated rocks: 10 Hz to 10 MHz," *Geophysics*, vol. 59, no. 6, pp. 909–917, Jun. 1994.
- [7] C. Portela, "Measurements and modeling of soil electromagnetic behavior," in *Proc. IEEE Int. Symp. Electromagn. Compat.*, Seattle, WA, USA, 1999, vol. 2, pp. 1004–1009.
- [8] R. Alipio and S. Visacro, "Modeling the frequency dependence of electrical parameters of soil," *IEEE Trans. Electromagn. Compat.*, vol. 56, no. 5, pp. 1163–1171, Oct. 2014.
- [9] Z. G. Datsios, P. N. Mikropoulos, and I. Karakousis, "Laboratory measurement of the low-frequency electrical properties of sand," in *Proc. 34th Int. Conf. Lightning Protection*, Rzeszow, Poland, 2018, pp. 1–6.
- [10] IEEE Guide for Measuring Earth Resistivity, Ground Impedance, and Earth Surface Potentials of a Grounding System, IEEE Std 81-2012 (Revision of IEEE Std 81-1983), pp. 1–86, 2012.
- [11] D. Clark et al., "Controlled large-scale tests of practical grounding electrodes—Part II: Comparison of analytical and numerical predictions with experimental results," *IEEE Trans. Power Del.*, vol. 29, no. 3, pp. 1240–1248, Jun. 2014.
- [12] N. Harid, D. Lathi, H. Griffiths, and A. Haddad, "Characterization of ground electrodes under low voltage variable frequency and impulse energization," in *Proc. Asia-Pacific Int. Conf. Lightning*, Nagoia, Japan, 2015, pp. 1–6.
- [13] H. Hasan, H. Hamzehbahmani, H. Griffiths, D. Guo, and A. Haddad, "Characterization of site soils using variable frequency and impulse voltages," in *Proc. 10th Asia-Pacific Int. Conf. Lightning*, Krabi, Thailand, 2017, pp. 1–4.
- [14] M. Geyab, A. A. Quadir, H. Griffiths, N. Harid, D. Clark, and A. Haddad, "Effect of current magnitude on measured apparent resistance of ground electrodes for 3 and 4-terminal low-voltage test configurations," in *Proc. Int. Conf. Grounding Earthing 8th Int. Conf. Lightning Phys. Effects*, Pirenópolis, Brazil, 2018, pp. 1–6.
- [15] J. Scott, "Electrical and magnetic properties of rock and soil," *U.S. Geological Surv., Dept. Interior*, Washington, DC, USA, 1966.
- [16] T. Ragheb and L. A. Geddes, "The polarization impedance of common electrode metals operated at low current density," *Annu. Biomed. Eng.*, vol. 19, pp. 151–163, 1991.
- [17] A. Revil, "Effective conductivity and permittivity of unsaturated porous materials in the frequency range 1 mHz-1GHz," *Water Resour. Res.*, vol. 49, no. 1, pp. 306–327, 2013.
- [18] A. D. B. Manjunath et al., "Investigation into variation of resistivity and permittivity of aqueous solutions and soils with frequency and current density," *IEEE Trans. Electromagn. Compat.*, vol. 64, no. 2, pp. 443–455, Apr. 2022, doi: [10.1109/TEMC.2021.3127640](https://doi.org/10.1109/TEMC.2021.3127640).
- [19] J. H. Scott, R. D. Carroll, and D. R. Cunningham, "Dielectric constant and electrical conductivity measurements of moist rock: A new laboratory method," *J. Geophys. Res.*, vol. 72, no. 20, pp. 5101–5115, 1967.
- [20] J. H. Scott, "Electrical and magnetic properties of rock and soil," U.S. Geological Surv., Denver, CO, USA, Open-File Rep. 83-915, 1983.
- [21] R. C. Bigelow and W. R. Eberle, "Empirical predicted curves for resistivity and conductivity of earth materials: 100 Hz to 100 MHz," U.S. Dept. Interior Geological Surv., Denver, CO, USA, Special project - 30, 1972.
- [22] S. Srinivasan, "Electrode/electrolyte interfaces: Structure and kinetics of charge transfer," in *Fuel Cells: From Fundamentals to Applications*. Berlin, Germany: Springer-Verlag, 2006, pp. 27–92.
- [23] F. Batalioto, A. R. Duarte, G. Barbero, and A. M. F. Neto, "Dielectric dispersion of water in the frequency range from 10 mHz to 30 MHz," *J. Phys. Chem.*, vol. 114, pp. 3467–3471, 2010.
- [24] E. T. McAdams, A. Lacknermeier, J. A. McLaughlin, D. Macken, and J. Jossinet, "The linear and non-linear electrical properties of the electrode-electrolyte interface," *Biosensors Bioelectron.*, vol. 10, pp. 67–74, 1995.
- [25] L. A. Geddes, "Historical evolution of circuit models for the electrode-electrolyte interface," *Annu. Biomed. Eng.*, vol. 25, pp. 1–14, 1997.
- [26] E. Warburg, "Ueber das verhalten sogenanter unpolarsbarer elektroden gegen wechselstroms," *Ann. Phys. Chim.*, vol. 67, pp. 493–499, 1899.
- [27] H. Fricke, "The theory of electrolytic polarization," *London, Edinburgh, Dublin Philos. Mag. J. Sci.*, vol. 14, no. 90, pp. 310–318, 1932.
- [28] T. Ragheb and L. A. Geddes, "Electrical properties of metallic electrodes," *Med. Biol. Eng. Comput.*, vol. 28, pp. 182–186, 1990.
- [29] L. A. Geddes and R. Roeder, "Measurement of the direct-current (Faradic) resistance of the electrode-electrolyte interface for commonly used electrode materials," *Ann. Biomed. Eng.*, vol. 29, no. 2, pp. 181–186, 2001.
- [30] E. E. Zimmerman, "The influence of temperature on polarization capacity and resistance," *Phys. Rev.*, vol. 35, pp. 543–553, 1930.
- [31] C. A. Dias, "Analytical model for a polarizable medium at radio and lower frequencies," *J. Geophys. Res.*, vol. 77, no. 26, pp. 4945–4956, 1972.
- [32] J. E. B. Randles, "Kinetics of rapid electrode reactions," *Discuss. Faraday Soc.*, vol. 1, pp. 11–19, Jan. 1947, doi: [10.1039/d9470100011](https://doi.org/10.1039/d9470100011).
- [33] B. B. Banerji, "The electrode capacity and resistance of electrolytes for a wide range of frequencies," *Trans. Faraday Soc.*, vol. 22, no. 9, pp. 111–132, Jan. 1926.
- [34] P. Córdoba-Torres, T. J. Mesquita, and R. P. Nogueira, "Relationship between the origin of constant-phase element behavior in electrochemical impedance spectroscopy and electrode surface structure," *J. Phys. Chem. C*, vol. 119, no. 8, pp. 4136–4147, Feb. 2015, doi: [10.1021/JP512063F](https://doi.org/10.1021/JP512063F).
- [35] P. Córdoba-Torres, T. J. Mesquita, and R. P. Nogueira, "Toward a better characterization of constant-phase element behavior on disk electrodes from direct impedance analysis: Methodological considerations and mass transport effects," *Electrochimica Acta*, vol. 92, pp. 323–334, Mar. 2013.
- [36] G. Y. Koga, B. Albert, V. Roche, and R. P. Nogueira, "On the intrinsic passivating ability of Belite-Ye'elimitite-Ferrite towards carbon steel: A straightforward comparison with ordinary Portland cement," *Corrosion Sci.*, vol. 147, pp. 141–151, Feb. 2019, doi: [10.1016/j.corsci.2018.11.012](https://doi.org/10.1016/j.corsci.2018.11.012).
- [37] G. R. Engelhardt, R. P. Case, and D. D. Macdonald, "Electrochemical impedance spectroscopy optimization on passive metals," *J. Electrochem. Soc.*, vol. 163, no. 8, pp. C470–C476, Jun. 2016, doi: [10.1149/2.0811608JES/XML](https://doi.org/10.1149/2.0811608JES/XML).

- [38] W. Zhang, X. Chen, Y. Wang, L. Wu, and Y. Hu, "Experimental and modeling of conductivity for electrolyte solution systems," *ACS Omega*, vol. 5, no. 35, pp. 22465–22474, Sep. 2020.
- [39] P. Gu, P. Xie, J. J. Beaudoin, and R. Brousseau, "A.C. impedance spectroscopy (I): A new equivalent circuit model for hydrated Portland cement paste," *Cement Concrete Res.*, vol. 22, no. 5, pp. 833–840, 1992.
- [40] G. Song, "Equivalent circuit model for AC electrochemical impedance spectroscopy of concrete," *Cement Concrete Res.*, vol. 30, no. 11, pp. 1723–1730, 2000.
- [41] B. Q. Dong et al., "Electrochemical impedance measurement and modeling analysis of the carbonation behavior for cementitious materials," *Construction Building Mater.*, vol. 54, pp. 558–565, Mar. 2014.
- [42] C. A. Dias, "Developments in a model to describe low-frequency electrical polarization of rocks," *Geophysics*, vol. 65, no. 2, pp. 437–451, 2000, doi: [10.1190/1.1444738](https://doi.org/10.1190/1.1444738).
- [43] P. J. Han, Y. F. Zhang, F. Y. Chen, and X. H. Bai, "Interpretation of electrochemical impedance spectroscopy (EIS) circuit model for soils," *J. Central South Univ.*, vol. 22, no. 11, pp. 4318–4328, 2015.
- [44] C. L. Longmire and H. J. Longley, "Time domain treatment of media with frequency-dependent electrical parameters," Defence Nucl. Agency, Washington, DC, USA, Rep. DNA 3167F, 1973.
- [45] H. J. Waxman and M. H. Vinegar, "Induced polarization of shaly sands," *Geophysics*, vol. 49, no. 8, pp. 1267–1287, 1984.
- [46] J.-L. Dellis, "Zfit," MATLAB Central File Exchange, 2020. Accessed: Mar. 2022. [Online]. Available: <https://www.mathworks.com/matlabcentral/fileexchange/19460-zfit>
- [47] W. Franks, I. Schenker, P. Schmutz, and A. Hierlemann, "Impedance characterization and modeling of electrodes for biomedical applications," *IEEE Trans. Biomed. Eng.*, vol. 52, no. 7, pp. 1295–1302, Jul. 2005.